

Experimental Detection of Qubit-Ququart Pseudo-Bound Entanglement using Three Nuclear Spins

Amandeep Singh,^{*} Akanksha Gautam,[†] Arvind,[‡] and Kavita Dorai[§]

*Department of Physical Sciences, Indian Institute of Science Education & Research Mohali,
Sector 81 SAS Nagar, Manauli PO 140306 Punjab India.*

In this work, we experimentally created and characterized a class of qubit-ququart PPT (positive under partial transpose) entangled states using three nuclear spins on an nuclear magnetic resonance (NMR) quantum information processor. Entanglement detection and characterization for systems with a Hilbert space dimension $\geq 2 \otimes 3$ is nontrivial since there are states in such systems which are both PPT as well as entangled. The experimental detection scheme that we devised for the detection of qubit-ququart PPT entanglement was based on the measurement of three Pauli operators with high precision, and is a key ingredient of the protocol in detecting entanglement. The family of PPT-entangled states considered in the current study are incoherent mixtures of five pure states. All the five states were prepared with high fidelities and the resulting PPT entangled states were prepared with mean fidelity ≥ 0.95 . The entanglement thus detected was validated by carrying out full quantum state tomography (QST).

PACS numbers: 03.67.Mn

I. INTRODUCTION

Quantum entanglement is one of the most counter-intuitive phenomena encountered in the quantum world and is at the heart of the quantum classical divide [1]. In the development of quantum information science, it was realized quite early that entanglement is a resource which can be exploited to achieve a quantum advantage for information processing and communication [2]. Specifically, entanglement has applications in quantum computing, quantum cryptography and key distribution [3, 4] and quantum teleportation [5]. Theoretically characterizing the entanglement of a given density operator has been one of the core research areas in quantum information processing [6]. While the entanglement characterization of pure bipartite quantum systems is well understood [7, 8], a complete characterization of mixed state entanglement remains elusive [9]. For mixed states, for two-qubit and qubit-qudit systems, the entanglement can be fully pinned down via the well known PPT (positive under partial transpose) criteria and such entanglement can also be distilled [10] into the form of EPR pairs [11]. However, for mixed states of quantum systems with Hilbert space dimensions greater than $2 \otimes 3$ and for multiparty situations, the problem of entanglement characterization is still an open question [12]. Entanglement exists in two fundamentally different forms [13, 14]: “free” entanglement which can be distilled into EPR pairs using local operations and classical communications (LOCC) [15] and “bound” entanglement which cannot be distilled into EPR pairs via LOCC.

Even in situations where entanglement can be characterized theoretically, the experimental detection of entanglement is resource-intensive and remains a challenging task [16, 17]. Several experimental efforts in this direction have tried to reduce the resources required to detect entanglement and have devised methods based on entanglement witnesses and positive maps to interrogate the presence of entanglement [18–22]. A range of experiments have been carried out to create and detect novel entangled states [23–30].

The term “bound” essentially implies that although correlations were established during the state preparation, they cannot be brought into a “free” form in terms of EPR pairs by a distillation process, and used wherever EPR pairs can be used as a resource. PPT entangled states are a prime example of bound entangled states and have been shown to be useful to establish a secret key [31], in the conversion of pure entangled states [32] and for quantum secure communication [33]. While the existence of “bound” entangled states has been proved beyond doubt, there are still only a few known classes of such states [13, 34–36]. The problem of finding all such PPT entangled states is still unsolved at the theoretical level.

Experimentally, bound entanglement has been created using four-qubit polarization states [37, 38] and entanglement unlocking of a four-qubit bound entangled state was also demonstrated [39]. Entanglement was characterized in bit-flip and phase-flip lossless quantum channel and the experiments were able to differentiate between free entangled, bound-entangled and separable states [40]. Continuous variable photonic bound-state entanglement has been created and detected in various experiments [41–43]. Two photon qutrit Bound-entangled states of two qutrits were investigated utilizing orbital angular momentum degrees of freedom [44]. In NMR, a three-qubit system was used to prepare a three-parameter pseudo-bound entangled state [45].

^{*} amandeepsingh@iisermohali.ac.in

[†] akankshagautam@iisermohali.ac.in

[‡] arvind@iisermohali.ac.in

[§] kavita@iisermohali.ac.in

In the present study, we experimentally create and characterize a one-parameter family of qubit-ququart PPT entangled states using three nuclear spins on a nuclear magnetic resonance (NMR) quantum information processor. There are a few proposals to detect PPT entanglement in the class of states introduced in Reference [13] by exploring local sum uncertainties [46] and by measuring individual spin magnetisation along different directions [47]. We chose the proposal of Reference [47] to experimentally detect PPT entanglement in states prepared on an NMR quantum information processor. The family of states considered in the current study is an incoherent mixture of five pure states and the relative strengths of the components of the mixture is controlled by a real parameter. We experimentally prepared different such PPT-entangled states, parameterized by a real parameter. These states represent five points on the one-parameter family of states. Discrete values of the real parameter were used which were uniformly distributed over the range for which the current detection protocol detects the entanglement. In order to experimentally detect entanglement in these states, three Pauli operators need to be measured in each case. To measure the required observables we utilized previously developed schemes [20–22] which unitarily map the desired state followed by NMR ensemble average measurements. In each case we also performed full quantum state tomography (QST) [48, 49] to verify the success of the detection protocol as well as to establish that the experimentally created states are indeed PPT entangled. Our work is important both in the context of preparing and characterizing bound entangled states and in devising new experimental schemes to detect PPT entangled states which use much fewer resources than are required by full quantum state tomography schemes. It should be noted here that we prepare the PPT entangled states using NMR in the sense that the total density operator for the spin ensemble always remains close to the maximally mixed state and at any given instance we are dealing with pseudo-entangled states [50].

This article is organized as follows: Sec. II characterizes bound entanglement in qubit-ququart systems and describes the theoretical aspects of the detection scheme. Sec. III contains the main results including the experimental NMR implementation of the PPT entanglement detection scheme. Sec. IV contains a few concluding remarks.

II. BOUND ENTANGLEMENT IN A QUBIT-QUQUART SYSTEM

Consider a 3-qubit quantum system with an eight-dimensional Hilbert space $\mathcal{H} = \mathcal{H}_1 \otimes \mathcal{H}_2 \otimes \mathcal{H}_3$, where \mathcal{H}_i represent qubit Hilbert spaces. If we choose to club the last two qubits into a single system with a four-dimensional Hilbert space $\mathcal{H}_q = \mathcal{H}_2 \otimes \mathcal{H}_3$, the three-qubit system can be reinterpreted as a qubit-ququart bipartite

system with Hilbert space $\mathcal{H} = \mathcal{H}_1 \otimes \mathcal{H}_q$. Formally we can say that the four ququart basis vectors $|e_i\rangle$ are mapped to the logical state vectors of the second and third qubits as $|e_1\rangle \leftrightarrow |00\rangle$, $|e_2\rangle \leftrightarrow |01\rangle$, $|e_3\rangle \leftrightarrow |10\rangle$ and $|e_4\rangle \leftrightarrow |11\rangle$ in the computational basis. With this understanding, we will freely use the three-qubit computational basis for this qubit-ququart system, where all along it is understood that the last two qubits form a ququart. For this system consider a family of PPT bound entangled states parameterized by a real parameter $b \in (0, 1)$ introduced by Horodecki [13].

$$\sigma_b = \frac{7b}{7b+1}\sigma_{\text{insep}} + \frac{1}{7b+1}|\phi_b\rangle\langle\phi_b| \quad (1)$$

with

$$\begin{aligned} \sigma_{\text{insep}} &= \frac{2}{7} \sum_{i=1}^3 |\psi_i\rangle\langle\psi_i| + \frac{1}{7}|011\rangle\langle 011|, \\ |\phi_b\rangle &= |1\rangle \otimes \frac{1}{\sqrt{2}} \left(\sqrt{1+b}|00\rangle + \sqrt{1-b}|11\rangle \right), \\ |\psi_1\rangle &= \frac{1}{\sqrt{2}}(|000\rangle + |101\rangle), \\ |\psi_2\rangle &= \frac{1}{\sqrt{2}}(|001\rangle + |110\rangle), \\ |\psi_3\rangle &= \frac{1}{\sqrt{2}}(|010\rangle + |111\rangle) \end{aligned} \quad (2)$$

It has been shown in [13] that the states in the family σ_b defined above are entangled for $0 < b < 1$ and is separable in the limiting cases $b = 0$ or 1 . One can explicitly write the density operator for the mixed PPT entangled states defined in Equation (1) in the computational basis as

$$\sigma_b = \frac{1}{1+7b} \begin{bmatrix} b & 0 & 0 & 0 & 0 & b & 0 & 0 \\ 0 & b & 0 & 0 & 0 & 0 & b & 0 \\ 0 & 0 & b & 0 & 0 & 0 & 0 & b \\ 0 & 0 & 0 & b & 0 & 0 & 0 & 0 \\ 0 & 0 & 0 & 0 & \frac{(1+b)}{2} & 0 & 0 & \frac{\sqrt{1-b^2}}{2} \\ b & 0 & 0 & 0 & 0 & b & 0 & 0 \\ 0 & b & 0 & 0 & 0 & 0 & b & 0 \\ 0 & 0 & b & 0 & \frac{\sqrt{1-b^2}}{2} & 0 & 0 & \frac{(1+b)}{2} \end{bmatrix} \quad (3)$$

It is interesting to observe that for $b = 0$, this family of states reduce to a separable state in $2 \otimes 4$ dimensions while it is still entangled in the three-qubit space and the entanglement is restricted to the two qubits forming the ququart.

Having defined the family of PPT entangled states in Equation(3) parameterized by ‘ b ’, we now describe the method that we use to experimentally detect their entanglement using a protocol proposed in Reference [47]. Although the family of states (3) is PPT entangled in $2 \otimes 4$ -dimensional Hilbert space, it is useful to exploit the underlying three-qubit structure. For the detection protocol, we define three observables B_i , with $i = 1, 2, 3$ (here B_1 acting on the qubit space and B_2 and B_3 act in

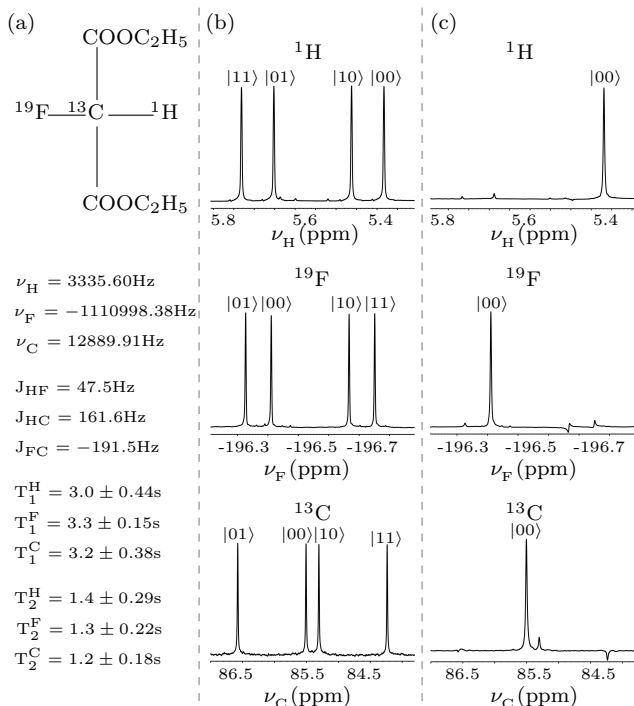


FIG. 1. (a) ^{13}C -labeled diethylfluoromalonate molecule and NMR parameters. NMR spectra of (b) thermal equilibrium state and (c) $|000\rangle$ pseudo pure state. Each transition is labeled with the logical states using the three-qubit basis

the state space of qubits 2 and 3 forming the ququart)

$$B_1 = \mathbb{I}_2 \otimes \sigma_x \otimes \sigma_x, \quad B_2 = \mathbb{I}_2 \otimes \sigma_y \otimes \sigma_y, \quad B_3 = \sigma_z \otimes \sigma_z \otimes \sigma_z \quad (4)$$

where $\sigma_{x,y,z}$ are the Pauli operators and \mathbb{I}_2 is the 2×2 identity operator. Although the observables B_j defined above are written in the three qubit notation, they are bona fide observables of the qubit-ququart system. The main result of Reference [47] is that any three-qubit separable state, ρ_s , obeys the four inequalities given by

$$|\langle B_1 \rangle_{\rho_s} \pm \langle B_2 \rangle_{\rho_s} \pm \langle B_3 \rangle_{\rho_s}| \leq 1 \quad (5)$$

Therefore, if a state violates even one of the four inequalities given in Eq. (5), it has to be entangled. It was shown numerically in [47] that the inequalities defined in Equation (5) can be used to detect the entanglement present in the states σ_b defined in Eq. (3) for $0 < b < \frac{1}{\sqrt{17}}$. Hence we are able to detect the entanglement of this family of PPT entangled in $2 \otimes 4$ dimensions.

III. EXPERIMENTAL DETECTION OF $2 \otimes 4$ BOUND ENTANGLEMENT

We now proceed toward experimentally preparing several different states from the family of states given by Eq. (3), detect them by measuring the observables de-

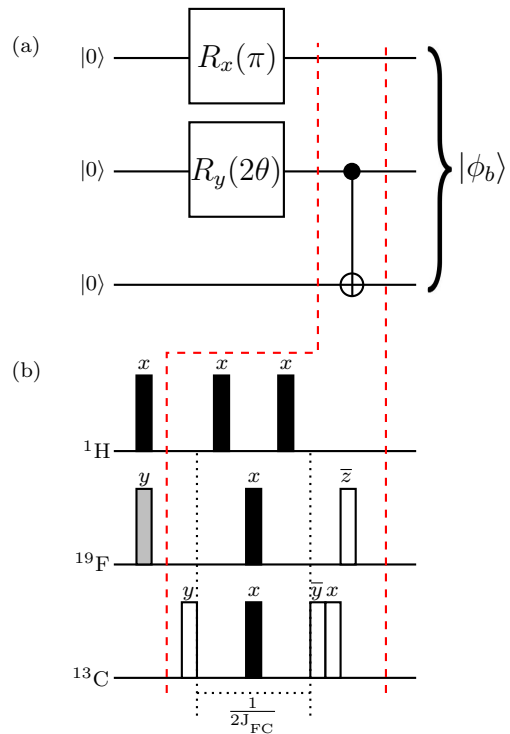


FIG. 2. (a) Quantum circuit to prepare $|\phi_b\rangle$ from $|000\rangle$ pseudopure state. (b) NMR pulse sequence for quantum circuit given in (a). Blank rectangles represent $\frac{\pi}{2}$ RF pulses, while black rectangles represent π spin-selective rotations. The gray rectangle represents a rotation through $\theta = \text{Cos}^{-1}\sqrt{1+b}/\sqrt{2}$. The phase of each RF pulse is written above the respective pulse. A bar over a phase implies negative phase, while the free evolution time interval is given by $(2J_{\text{FC}})^{-1}$.

fined in Eq. (4) and check if we observe a violation of the inequalities defined in Eq. (5).

In order to prepare the PPT entangled family of states in $2 \otimes 4$ dimensions using three qubits, we chose three spin-1/2 nuclei (^1H , ^{19}F and ^{13}C) to encode the three qubits in a ^{13}C -labeled sample of diethylfluoromalonate dissolved in acetone- D_6 . The weak-field free evolution NMR Hamiltonian for the system is given by [51]

$$\mathcal{H} = -\sum_{i=1}^3 \nu_i I_{iz} + \sum_{i>j,i=1}^3 J_{ij} I_{iz} I_{jz} \quad (6)$$

where the indices $i, j = 1, 2$ or 3 label the qubit, ν_i are the respective chemical shifts, I_{iz} is the Pauli z spin angular momentum operator of the i^{th} spin and J_{ij} is the scalar spin-spin coupling strength. The ensemble was first initialized in the pseudopure state (PPS) $|000\rangle$ using the spatial averaging method with the PPS density operator being given by [52]

$$\rho_{000} = \frac{(1-\epsilon)}{2^3} \mathbb{I}_8 + \epsilon |000\rangle\langle 000| \quad (7)$$

where ϵ ($\sim 10^{-5}$) is the thermal spin magnetization given by the Boltzmann factor ($\mu\text{B}/k_{\text{B}}\text{T}$) of the spin ensemble

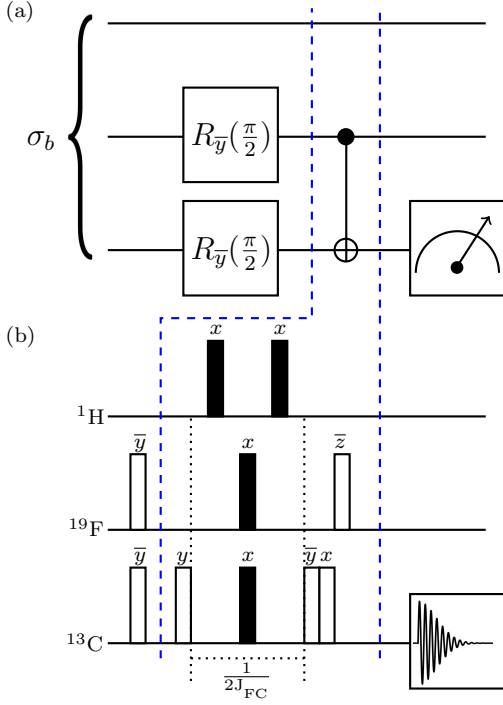


FIG. 3. (a) Quantum circuit to map σ_b to the state σ'_b such that $\langle B_1 \rangle_{\sigma_b} = \langle I_{3z} \rangle_{\sigma'_b}$. (b) NMR pulse sequence to achieve the quantum circuit in (a). The unfilled rectangles denote $\frac{\pi}{2}$ RF pulses, while the filled rectangles represent π spin-selective RF pulses. The phase of each RF pulse is written above the respective pulse. A bar over a phase implies negative phase and the free evolution time interval is given by $\frac{1}{2J_{FC}}$.

placed in a static magnetic field B at temperature T and \mathbb{I}_8 is the 8×8 identity operator. The NMR experimental parameters as well as the spectra of the thermal and PPS states are shown in Fig.(1). Each transition in the NMR spectra is labeled with the logical state of the passive qubits. We experimentally prepared the PPS with a fidelity of 0.98 ± 0.01 . The state fidelity was computed using the fidelity measure [53, 54]

$$F = \left[\text{Tr} \left(\sqrt{\sqrt{\rho_{\text{th}}} \rho_{\text{ex}} \sqrt{\rho_{\text{th}}}} \right) \right]^2, \quad (8)$$

where ρ_{th} and ρ_{ex} represent theoretically expected and experimentally prepared density operators, respectively and F is normalized in the sense that $F \rightarrow 1$ as $\rho_{\text{ex}} \rightarrow \rho_{\text{th}}$.

The experimentally prepared bound entangled states in the current study were directly detected using the protocol discussed in Sec. II and full QST [48] was also performed in each case to verify the results. QST utilized a set of seven preparatory pulses $\{III, XXX, IYY, XYX, YII, XXY, IYY\}$, where I implies ‘no-operation’ and $X(Y)$ is a local $\frac{\pi}{2}$ unitary rotation with phase $x(y)$. In NMR, such local unitary rotations are achieved using highly accurate and calibrated

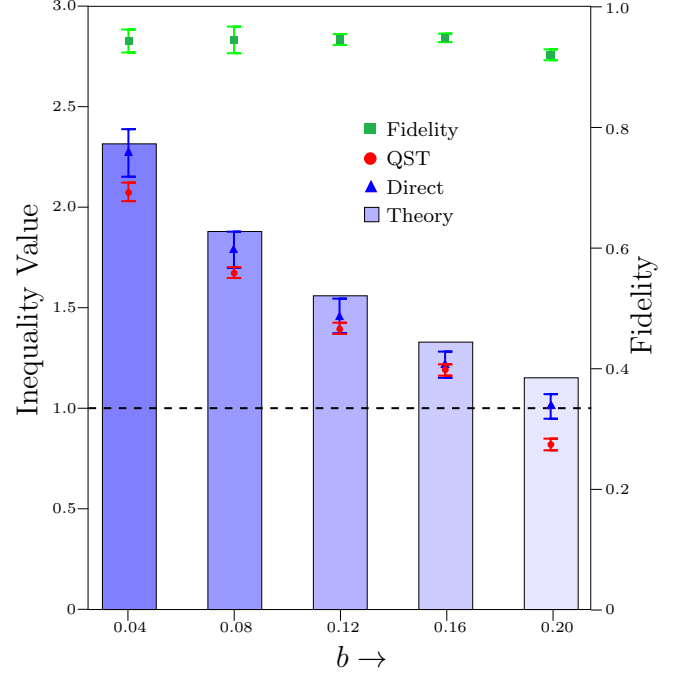


FIG. 4. (Color online) Bars represent theoretically expected values, red circles are the values obtained via QST and blue triangles are the direct experimental values for the inequality appearing in Eq.(4). Green squares are the mean experimental fidelities. Horizontal black dashed line is the reference line for states in Eq.(1) violating inequality of Eq.(4).

spin-selective radiofrequency (RF) pulses applied transverse to the static magnetic field. Experiments were performed on a Bruker Avance-III 600 MHz FT-NMR spectrometer equipped with QXI probe at room temperature ($\sim 20^\circ\text{C}$). Three dedicated channels for ^1H , ^{19}F and ^{13}C nuclei were employed having $\frac{\pi}{2}$ RF pulse durations of $9.33 \mu\text{s}$, $22.55 \mu\text{s}$ and $15.90 \mu\text{s}$ at the power levels of 18.14 W , 42.27 W and 179.47 W respectively.

The next step was to prepare the PPT entangled family of states given in Eq. (3) (each with a fixed value of the parameter b) and to achieve this we utilized the method of temporal averaging [52]. The family of states σ_b is an incoherent mixture of several pure states as given in Equation(2), and the quantum circuit to prepare one such nontrivial state ($|\phi_b\rangle$) is given in Fig.2(a), where $R_x(\pi)$ represents a local unitary rotation through an angle π with a phase x . After experimentally preparing the state, one can measure the desired observable in Eq. (4), by mapping the state onto the Pauli basis operators. The quantum circuit to achieve this is shown in Fig.3(a), and this circuit maps the state $\sigma_b \rightarrow \sigma'_b$ such that $\langle B_1 \rangle_{\sigma_b} = \langle I_{3z} \rangle_{\sigma'_b}$. The motivation for such a mapping [20–22] relies on the fact that in an NMR scenario, the expectation value $\langle I_z \rangle$, can be readily measured [51]. The crux of the temporal averaging technique relies on the fact that the five states composing the PPT entangled

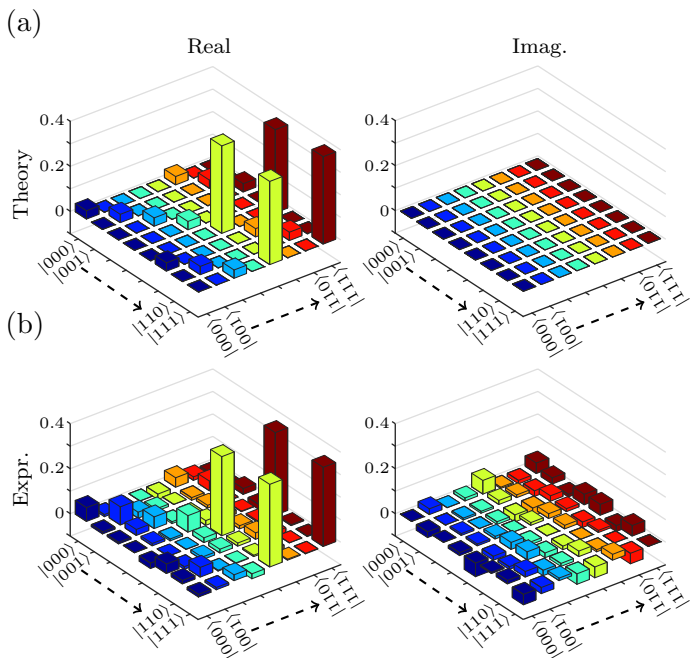


FIG. 5. Real and imaginary parts of the tomograph of the (a) theoretically expected and (b) experimentally reconstructed density operator for PPT entangled state with $b = 0.04$ and state fidelity $F=0.968$.

state are generated via five different experiments. The states of these experiments are then added with appropriate probabilities to achieve the desired PPT entangled state.

All the five states, appearing in Eq.(2), *i.e.* $|\phi_b\rangle$, $|\psi_1\rangle$, $|\psi_2\rangle$, $|\psi_3\rangle$ and the separable PPS state $|011\rangle$ were experimentally prepared with state fidelities ≥ 0.96 . It is worthwhile to note here that $|\phi_b\rangle$ is a generalized biseparable state while $|\psi_1\rangle$ and $|\psi_3\rangle$ are LOCC equivalent biseparable states with maximal entanglement between the first and third qubits and $|\psi_2\rangle$ is a state belonging to the GHZ class. For the experimental demonstration of the detection protocol discussed in Sec.II we chose the values $b = 0.04, 0.08, 0.12, 0.16$ and 0.20 and prepared five different PPT entangled states. The quantum circuit as well as the NMR pulse sequence to prepare $|\phi_b\rangle$ is shown in Fig.(2). Other states in Eq.(2) have similar circuits as well as pulse sequences and are not shown here. The tomograph for one such experimentally prepared PPT entangled state, with $b = 0.04$ and fidelity $F = 0.968$, is shown in Fig.(5). In order to measure the expectation values of the observables appearing in Eq.(4) we utilized the procedure developed in our earlier work [20, 21]. The idea is to unitarily map the state σ_b to a state say σ'_b , such that $\langle \mathbb{O} \rangle_{\sigma_b} = \langle I_{iz} \rangle_{\sigma'_b}$ where \mathbb{O} is one of the observables to be measured in the state σ_b . This is achieved by measuring I_{iz} on σ'_b . As an example, one can find the expectation value $\langle B_1 \rangle_{\sigma_b}$ using the quantum circuit given in Fig.3(a) and the NMR pulse sequence given in Fig.3(b) is implemented, followed by

a measurement of the spin magnetization of the third qubit. Such a normalized magnetization of a qubit in the mapped state is indeed proportional to the expectation value of the z -spin angular momentum of the qubit [51]. Experimentally measured values of the inequality given

TABLE I. Experimentally measured values of the inequality in Eq. (5) showing maximum violation for five different PPT entangled states.

Obs. \rightarrow State(F) \downarrow	b	Inequality value from:		
		Theory	QST	Experimental
$\sigma_{b_1}(0.946 \pm 0.019)$	0.04	2.311	2.061 ± 0.046	2.269 ± 0.118
$\sigma_{b_2}(0.947 \pm 0.022)$	0.08	1.876	1.660 ± 0.027	1.784 ± 0.090
$\sigma_{b_3}(0.949 \pm 0.009)$	0.12	1.557	1.382 ± 0.028	1.451 ± 0.086
$\sigma_{b_4}(0.953 \pm 0.007)$	0.16	1.327	1.179 ± 0.028	1.213 ± 0.065
$\sigma_{b_5}(0.925 \pm 0.009)$	0.20	1.150	0.807 ± 0.029	1.007 ± 0.061

in Eq. 5 with maximum violation are reported in Table-I. For all five states with different b values, full QST was also performed and the observables 4 were analytically computed from the reconstructed density operators. All the experimental results, tabulated in the Table-I, are plotted in Fig. (4). Blue bars represent the theoretically expected values, red circles are the values obtained via full QST and blue triangles are the direct experimental values for the inequality appearing in Eq.(4). Green squares are the mean experimental fidelities. Horizontal black dashed line is the reference line for states in Eq.(1) violating inequality of Eq.(4). All the experiments were performed several times to ensure the reproducibility of the experimental results as well as to estimate the errors reported in Table I. It was observed that the experimental values, within experimental error limits, agree well with theoretically expected values and validate the success of the detection protocol in identifying the PPT entangled family of states. The direct QST based measurements of the state also validate our experimental results.

IV. CONCLUDING REMARKS

The characterization of bound entangled states is useful since it sheds light on the relation between intrinsically quantum phenomena such as entanglement and nonlocality. The detection of bound entangled states is theoretically a hard task and there are as yet no simple methods to characterize all such states for arbitrary composite quantum systems. The structure of PPT entangled states is rather complicated and does not easily lead to a simple parametrization in terms of a noise parameter. In this work, we have reported the experimental creation of a family of PPT entangled states of a qubit-ququart system and the implementation of a detection protocol involving local measurements to detect their bound entanglement. Five different states which were parameterized by a real parameter ' b ', were ex-

perimentally prepared (with state fidelities ≥ 0.95) to represent the PPT entangled family of states. All the experiments were repeated several times to ensure the reproducibility of the experimental results and error estimation. In each case we observed that the detection protocol successfully detected the PPT entanglement of the state in question within experimental error limits. The results were further substantiated via full QST for each prepared state. It would be interesting to create the PPT entangled family of states using different pseudopure creation techniques and in higher dimensions, and these directions will be taken up in future work.

ACKNOWLEDGMENTS

All the experiments were performed on a Bruker Avance-III 600 MHz FT-NMR spectrometer at the NMR Research Facility of IISER Mohali. Arvind acknowledges funding from DST India under Grant No. EMR/2014/000297. K.D. acknowledges funding from DST India under Grant No. EMR/2015/000556.

-
- [1] E. Schrödinger, *Naturwissenschaften* **23**, 807 (1935).
- [2] M. A. Nielsen and I. L. Chuang, *Quantum Computation and Quantum Information* (Cambridge University Press, 2000).
- [3] C. H. Bennett, F. Bessette, G. Brassard, L. Salvail, and J. Smolin, *Journal of Cryptology* **5**, 3 (1992).
- [4] S. P. Walborn, D. S. Lemelle, M. P. Almeida, and P. H. S. Ribeiro, *Phys. Rev. Lett.* **96**, 090501 (2006).
- [5] M. Riebe, H. Häffner, C. F. Roos, W. Hänsel, J. Benhelm, G. P. T. Lancaster, T. W. Körber, C. Becher, F. Schmidt-Kaler, D. F. V. James, and R. Blatt, *Nature* **429**, 734 (2004).
- [6] R. Horodecki, P. Horodecki, M. Horodecki, and K. Horodecki, *Rev. Mod. Phys.* **81**, 865 (2009).
- [7] A. Peres, *Phys. Rev. Lett.* **77**, 1413 (1996).
- [8] M. Horodecki, P. Horodecki, and R. Horodecki, *Phys. Lett. A* **223**, 1 (1996).
- [9] M. Horodecki, P. Horodecki, and R. Horodecki, “Mixed-state entanglement and quantum communication,” in *Quantum Information* (Springer, Berlin, Heidelberg, 2001) pp. 151–195.
- [10] C. H. Bennett, H. J. Bernstein, S. Popescu, and B. Schumacher, *Phys. Rev. A* **53**, 2046 (1996).
- [11] M. Horodecki, P. Horodecki, and R. Horodecki, *Phys. Rev. Lett.* **78**, 574 (1997).
- [12] O. Gühne and G. Tóth, *Phys. Rep.* **474**, 1 (2009).
- [13] P. Horodecki, *Phys. Lett. A* **232**, 333 (1997).
- [14] M. Horodecki, P. Horodecki, and R. Horodecki, *Phys. Rev. Lett.* **80**, 5239 (1998).
- [15] M. A. Nielsen, *Phys. Rev. Lett.* **83**, 436 (1999).
- [16] C. Spengler, M. Huber, S. Brierley, T. Adaktylos, and B. C. Hiesmayr, *Phys. Rev. A* **86**, 022311 (2012).
- [17] J. Dai, Y. L. Len, Y. S. Teo, B.-G. Englert, and L. A. Krivitsky, *Phys. Rev. Lett.* **113**, 170402 (2014).
- [18] J. G. Filgueiras, T. O. Maciel, R. E. Aucasse, R. O. Vianna, R. S. Sarthour, and I. S. Oliveira, *Quantum Information Processing* **11**, 1883 (2012).
- [19] Q. Yu, Y. Zhang, J. Li, H. Wang, X. Peng, and J. Du, *Sci. China-Phys. Mech. Astron.* **60**, 070313 (2017).
- [20] A. Singh, Arvind, and K. Dorai, *Phys. Rev. A* **94**, 062309 (2016).
- [21] A. Singh, H. Singh, K. Dorai, and Arvind, *Phys. Rev. A* **98**, 032301 (2018).
- [22] A. Singh, K. Dorai, and Arvind, *Quantum Information Processing* **17**, 334 (2018).
- [23] D. Bouwmeester, J.-W. Pan, M. Daniell, H. Weinfurter, and A. Zeilinger, *Phys. Rev. Lett.* **82**, 1345 (1999).
- [24] C. F. Roos, M. Riebe, H. Häffner, W. Hänsel, J. Benhelm, G. P. T. Lancaster, C. Becher, F. Schmidt-Kaler, and R. Blatt, *Science* **304**, 1478 (2004).
- [25] M. Bourennane, M. Eibl, C. Kurtsiefer, S. Gaertner, H. Weinfurter, O. Gühne, P. Hyllus, D. Bruß, M. Lewenstein, and A. Sanpera, *Phys. Rev. Lett.* **92**, 087902 (2004).
- [26] D. Leibfried, E. Knill, S. Seidelin, J. Britton, R. B. Blakestad, J. Chiaverini, D. B. Hume, W. M. Itano, J. D. Jost, C. Langer, R. Ozeri, R. Reichle, and D. J. Wineland, *Nature* **438**, 639 (2005).
- [27] H. Häffner, W. Hänsel, C. F. Roos, J. Benhelm, D. Chekhal kar, M. Chwalla, T. Körber, U. D. Rapol, M. Riebe, P. O. Schmidt, C. Becher, O. Gühne, W. Dür, and R. Blatt, *Nature* **438**, 643 (2005).
- [28] D. Das, S. Dogra, K. Dorai, and Arvind, *Phys. Rev. A* **92**, 022307 (2015).
- [29] S. Dogra, K. Dorai, and Arvind, *Phys. Rev. A* **91**, 022312 (2015).
- [30] H. Singh, Arvind, and K. Dorai, *Phys. Rev. A* **97**, 022302 (2018).
- [31] K. Horodecki, M. Horodecki, P. Horodecki, and J. Oppenheim, *Phys. Rev. Lett.* **94**, 160502 (2005).
- [32] S. Ishizaka, *Phys. Rev. Lett.* **93**, 190501 (2004).
- [33] Y. Zhou, J. Yu, Z. Yan, X. Jia, J. Zhang, C. Xie, and K. Peng, *Phys. Rev. Lett.* **121**, 150502 (2018).
- [34] J. A. Smolin, *Phys. Rev. A* **63**, 032306 (2001).
- [35] A. Acín, D. Bruß, M. Lewenstein, and A. Sanpera, *Phys. Rev. Lett.* **87**, 040401 (2001).
- [36] R. Sengupta and Arvind, *Phys. Rev. A* **84**, 032328 (2011).
- [37] E. Amselem and M. Bourennane, *Nat. Phys.* **5**, 748 (2009).
- [38] F. Kaneda, R. Shimizu, S. Ishizaka, Y. Mitsumori, H. Kosaka, and K. Edamatsu, *Phys. Rev. Lett.* **109**, 040501 (2012).
- [39] J. Lavoie, R. Kaltenbaek, M. Piani, and K. J. Resch, *Phys. Rev. Lett.* **105**, 130501 (2010).
- [40] E. Amselem, M. Sadiq, and M. Bourennane, *Sci. Rep.* **3**, 1966 (2013).
- [41] K. Dobek, M. Karpiski, R. Demkowicz-Dobrzanski, K. Banaszek, and P. Horodecki, *Laser Phys.* **23**, 025204 (2013).
- [42] J. DiGuglielmo, A. Sambrowski, B. Hage, C. Pineda, J. Eisert, and R. Schnabel, *Phys. Rev. Lett.* **107**, 240503 (2011).

- (2011).
- [43] F. E. S. Steinhoff, M. C. de Oliveira, J. Sperling, and W. Vogel, Phys. Rev. A **89**, 032313 (2014).
- [44] B. C. Hiesmayr and W. Löffler, New J. Phys. **15**, 083036 (2013).
- [45] H. Kampermann, D. Bruß, X. Peng, and D. Suter, Phys. Rev. A **81**, 040304 (2010).
- [46] M.-J. Zhao, T.-G. Zhang, X. Li-Jost, and S.-M. Fei, Phys. Rev. A **87**, 012316 (2013).
- [47] Y. Akbari-Kourbolagh, Int. J. Quan. Info. **15**, 1750049 (2017).
- [48] G. M. Leskowitz and L. J. Mueller, Phys. Rev. A **69**, 052302 (2004).
- [49] H. Singh, Arvind, and K. Dorai, Phys. Lett. A **380**, 3051 (2016).
- [50] R. Laflamme, E. Knill, W. Zurek, P. Catasti, and S. Mariappan, Philos. Trans. R. Soc. A **356**, 1941 (1998).
- [51] R. R. Ernst, G. Bodenhausen, and A. Wokaun, *Principles of NMR in One and Two Dimensions* (Clarendon Press, 1990).
- [52] D. G. Cory, M. D. Price, and T. F. Havel, Physica D: Nonlinear Phenomena **120**, 82 (1998).
- [53] A. Uhlmann, Rep. Math. Phys. **9**, 273 (1976).
- [54] R. Jozsa, J. Mod. Optics **41**, 2315 (1994).